Edge-to-center density ratios in low-temperature plasmas

2015 Plasma Sources Sci. Technol. 24 025017

(http://iopscience.iop.org/0963-0252/24/2/025017)

IOP Publishing Plasma Sources Science and Technology
Plasma Sources Sci. Technol. **24** (2015) 025017 (6pp) doi:10.1088/0963-0252/24/2/025017

Edge-to-center density ratios in low-temperature plasmas

T Lafleur[1,2] **and P Chabert**[1]

[1] Laboratoire de Physique des Plasmas, CNRS, Sorbonne Universités, UPMC Univ Paris 06, Univ Paris-Sud, Ecole Polytechnique, 91128 Palaiseau, France
[2] ONERA-The French Aerospace Lab, 91120 Palaiseau, France

E-mail: trevor.lafleur@lpp.polytechnique.fr

Received 15 December 2014, revised 13 January 2015
Accepted for publication 26 January 2015
Published 2 March 2015

Abstract

The ion flux leaving a plasma at a boundary can be given by: $\Gamma_i = h_L n_0 u_B$, where n_0 is the maximum central plasma density, u_B is the Bohm velocity, and h_L is the sheath edge-to-center plasma density ratio. Such h_L factors have become synonymous with global modeling of plasma discharges, where they play a vital role in the prediction of plasma losses to bounding surfaces. By performing one-dimensional (1D) particle-in-cell simulations of inductively and capacitively coupled plasmas (ICPs and CCPs) over a wide pressure range, we explicitly test the validity of standard heuristic formulae commonly used to estimate h_L. The ICP simulation results are found to be in very good agreement, while a large discrepancy is present for the CCP results at high pressures. The onset of this discrepancy is found to be correlated with the bulk-to-sheath edge ionization transition that occurs in CCPs at high pressures. Consequently, global models will strongly underestimate plasma losses in this regime.

Keywords: particle-in-cell, sheath edge-to-center density ratios, plasma transport, global models

(Some figures may appear in colour only in the online journal)

1. Introduction

In almost all low-temperature bounded plasmas a sheath exists near the plasma edges, separating the bulk quasi-neutral plasma region from the boundary surfaces. These sheaths are nominally established to provide some form of charged particle flux continuity, and in the case of insulating or floating boundaries, ensure equal fluxes of electrons and positive ions to the walls. For a stable sheath to form it is necessary for ions to enter with a velocity larger than or equal to the Bohm velocity, which necessitates a region before the sheath (known as the presheath) in which ions are accelerated to this velocity. This ion acceleration then results in a decrease in density from the central plasma region to the sheath edge (for a more detailed discussion on plasma sheaths, see for example [1, 2]).

The decrease of plasma density in the presheath leads to an important quantity in low-temperature gas discharge modeling: the sheath edge-to-center density ratio, $h_L = n_s/n_0$ (where n_s and n_0 are the densities at the sheath edge and center respectively). This ratio is particularly relevant to global models [3–5], which represent some of the simplest models used to predict plasma parameters and scaling laws. Such models also form indispensible tools in plasmas with very complex chemistries, where fluid or kinetic simulations are either too time consuming to perform, or too difficult to extract useful parameter trends. Global models have been used to predict the behavior of many different types of plasma discharges, including capacitively coupled plasmas (CCPs) [6–12], inductively coupled plasmas (ICPs) [13–18], helicon [19, 20] and microwave [21] discharges, plasma thrusters such as ion engines [22, 23], and with many different gases (including gas mixtures) [24–27] in these discharges.

The edge-to-center density ratios are essential in estimating the correct plasma losses to boundary surfaces; both particle losses, and power losses. In its simplest form, the particle balance (per unit cross-sectional area) of a one-ion-species unmagnetized plasma in a 1D planar geometry can be given by

$$2h_L n_0 u_B = n_0 n_g K_{iz} L \quad (1)$$

Table 1. Range of plasma parameters tested in the simulation cases.

Simulation case	d/λ_i	λ_{De0} (mm)	T_e (eV)
Argon ICP (13.56 MHz)	0–298	0.2–0.6	2.8–5.3
Argon CCP (13.56 MHz)	18–428	0.1–0.2	1.1–3.4
Argon CCP (60 MHz)	0.8–365	0.2–0.5	3.6–4.2
Helium ICP (13.56 MHz)	0–343	0.3–2	4.3–19.3
Helium CCP (13.56 MHz)	46–681	0.3–0.6	3.7–4.7

where $u_B = \sqrt{\frac{qT_e}{M}}$ is the Bohm velocity with q the ion charge, T_e the electron temperature and M the ion mass, L is the length of the discharge, n_g is the neutral gas density, and K_{iz} is the ionization rate factor. The left-hand side (LHS) of equation (1) represents the particle losses to the walls, while the right-hand side (RHS) represents particle production due to ionization. The h_L ratio here reflects the fact that the ion density at the sheath edge is lower than that in the bulk plasma, and is thus important for estimating the true ion flux loss to the walls, which would otherwise be strongly overestimated. A somewhat similar equation to equation (1) also exists for the plasma power balance [4, 5].

A number of authors have performed theoretical work to provide useful formulae for the plasma density profiles (and hence h_L factors) in low-temperature discharges. The low pressure ($\lambda_i/L \gg 1$, where λ_i is the ion–neutral mean free path) limit was first treated by Tonks and Langmuir [28], while the opposite high pressure ($\lambda_i/L \ll 1$) limit was considered by Schottky [29] (who set the density at the boundaries to zero, and so $h_L = 0$). This original treatment by Schottky has subsequently been modified to account for a non-zero plasma density at the walls [4, 5]. In the intermediate pressure regime, which is typically the regime of interest in most industrial plasmas, Godyak [3], and more recently Raimbault and Chabert [30], have obtained useful approximate formulae. A commonly used heuristic fit to the above three pressure regimes has been proposed in [5]

$$h_L \approx 0.86\left[3 + \frac{1}{2}\frac{d}{\lambda_i} + \frac{1}{5}\frac{T_i}{T_e}\left(\frac{d}{\lambda_i}\right)^2\right]^{-1/2} \quad (2)$$

where T_i is the ion temperature. This formula has recently been confirmed [31] using a detailed one-dimensional fluid model including both a nonzero ion temperature, as well as the ion inertial terms in the momentum balance equation.

In most of the theoretical models mentioned above, there are a number of important assumptions used in order to obtain analytical solutions. These include: (1) temporal variations in plasma parameters are negligible, (2) electrons follow the Boltzmann relation and are isothermal, (3) the ionization rate factor, $K_{iz} = K_{iz}(T_e)$, depends only on a spatially and temporally constant electron temperature, T_e, and (4) secondary electron emission from boundaries is not considered. However, global models and h_L ratios are predominantly used in rf plasmas, where many of these assumptions are not necessarily valid. This is particularly true for CCPs, where it is well known that there are strong rf modulations of the plasma parameters, and where the ionization rate can be strongest near the expanding sheaths [4]. Experimental verification of formulae such as equation (2) has also been very limited [32], due to the need for multiple measurements which can increase errors significantly. In this short paper we explicitly test equation (2) by using 1D particle-in-cell (PIC) simulations, where none of the assumptions (1)–(4) need be made. We test equation (2) over a wide pressure range, using PIC simulations that model both CCP and ICP discharges.

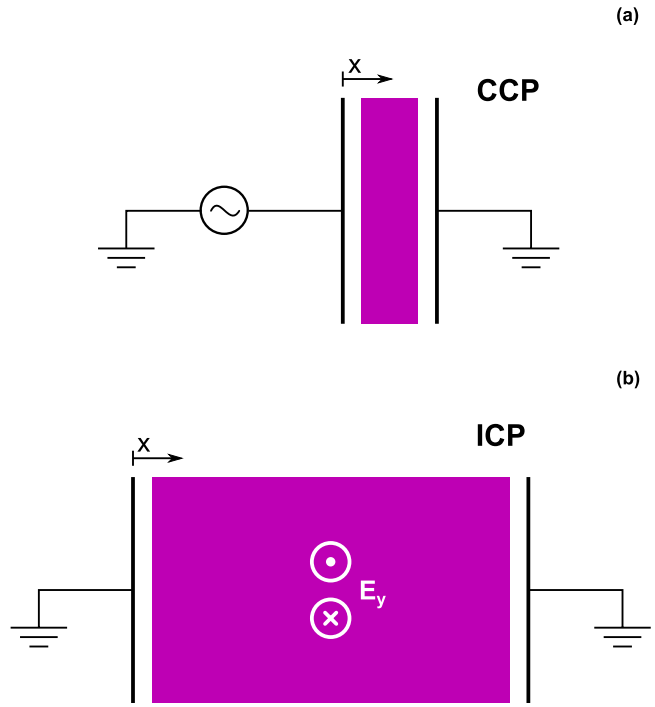

Figure 1. Schematic of the (*a*) CCP, and (*b*) ICP PIC simulation models. For the ICP model, a transverse time-varying electric field (into/out-of the page) is uniformly applied throughout the simulation region.

2. PIC simulation description

A schematic of the 1D CCP and ICP PIC simulations used is shown in figure 1. The CCP simulation code has been previously described and benchmarked in [33–35]. Here the RHS electrode is grounded, while the LHS electrode is powered by an rf voltage or current-driven source. The majority of simulations are performed using argon gas, which is assumed to be spatially uniform with a temperature of 300 K. A limited number of simulations are also performed using helium, which are based on the CCP benchmark tests described in [35]. Electron–neutral collision cross-sections (including ionization, excitation, and elastic scattering reactions) are taken from [37] for argon, and [39] for helium, while ion–neutral cross-sections (including charge-exchange and elastic scattering reactions) are taken from [38] and [40] for argon and helium respectively. For the argon simulations, the powered electrode is current-driven with an amplitude of 25.6 Am^{-2}, and at frequencies of either 13.56 MHz (to simulate the well known experiments of Godyak and Piejak [41]) or 60 MHz. The gap length is 2 cm. The 13.56 MHz

simulations have a secondary electron emission coefficient due to ion bombardment, γ, of 0.1, while electrons are reflected with a probability of 0.2. For the helium simulations the powered electrode is voltage-driven at 13.56 MHz, the amplitude of which changes at different pressures to give a constant discharge current amplitude of about 10 Am^{-2}. The gap length for the helium simulations is larger at 6.7 cm.

The ICP code is similar to that described in [36]. Here both the LHS and RHS electrodes are grounded, and the discharge is maintained via an rf electric field applied transverse to the simulation direction, which models the inductive fields from an rf antenna. The strength of this electric field is modified at each time step so as to ensure a sinusoidally varying transverse 'discharge' current [36]. For both the CCP and ICP simulations, we use about 100 000 particles for each particle species, and the time step and grid spacing is set to satisfy the usual stability/accuracy criteria [35].

3. Results

As discussed in section 1, the ion flux lost to a boundary surface is usually given as $\Gamma_\mathrm{i} = h_\mathrm{L} n_0 u_\mathrm{B}$. Although h_L is nominally the edge-to-center density ratio, ionization can also occur in the sheaths. For global modeling of discharges it is usually the total ion flux that reaches the boundaries which is important, not just the ion flux at the sheath edges. This is because any additional ionization inside the sheaths will increase the ion flux and hence also the particle and power losses. Therefore, in the simulation results to follow, we define h_L as

$$h_\mathrm{L} = \frac{\Gamma_\mathrm{i}}{n_0 u_\mathrm{B}} \tag{3}$$

where Γ_i is the time-averaged (over an rf period) ion flux at the boundaries, n_0 is the maximum central plasma density, and $u_\mathrm{B} = \sqrt{qT_\mathrm{e}/M}$ is the Bohm velocity with T_e the time and space-averaged electron temperature. In the theoretical formula for h_L (i.e. equation (2)), the length d is not the discharge length, but rather the length of the bulk quasi-neutral plasma region between the plasma sheaths. This quasi-neutral region is defined as $d = L - 2s$, where L is the geometric length of the discharge, and s is the sheath width (defined as the location where $|n_\mathrm{i} - n_\mathrm{e}|/n_\mathrm{i} = 1\%$). In most of the simulations, $T_\mathrm{i}/T_\mathrm{e} \sim 0.01$–$0.02$. The ion–neutral mean free path, $\lambda_\mathrm{i} = 1/n_\mathrm{g}\sigma_\mathrm{i}$, is found by calculating the neutral gas density from the known simulation pressure, and using a representative value of the ion–neutral collision cross-section, which is about $1 \times 10^{-18}\,\mathrm{m}^2$ for argon, and $4 \times 10^{-19}\,\mathrm{m}^2$ for helium. The range of plasma parameters tested in the simulations is shown in table 1.

Figure 2 shows a comparison of the PIC simulation results with equation (2) for both argon and helium. The last LHS point of each PIC result represents the lower pressure limit where a discharge can be ignited/sustained. The far left ICP points at $d/\lambda_\mathrm{i} = 0.1$ were obtained at a higher pressure (to allow a discharge to be sustained) but with ion–neutral collisions turned off (the point has been moved for convenience from $d/\lambda_\mathrm{i} = 0$ to 0.1). Due to statistical noise, and uncertainty in the sheath edge location, the PIC simulation results have

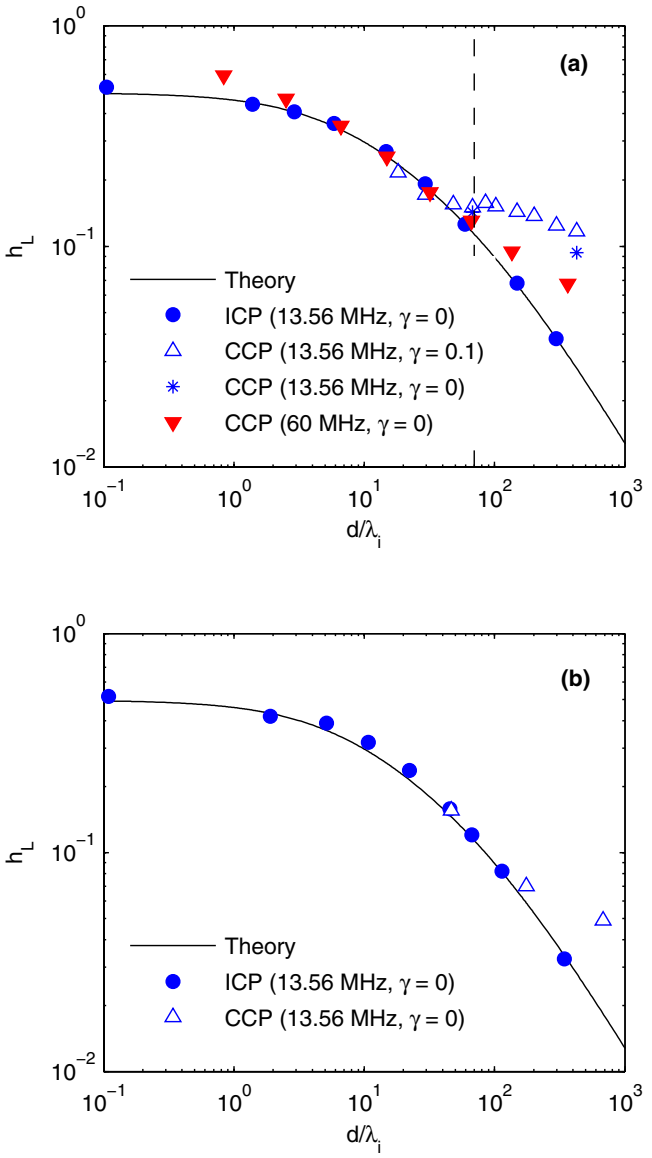

Figure 2. Edge-to-center plasma density ratios for the CCP and ICP PIC simulations using (*a*) argon, and (*b*) helium. The solid curves in (*a*) and (*b*) show the theoretical values from equation (2) (with $T_\mathrm{i}/T_\mathrm{e} = 0.02$), while the vertical dashed line in (*a*) approximately denotes the value of d/λ_i where the bulk-to-edge ionization transition occurs in the CCP simulations.

an uncertainty of about 5–10%. As seen, the ICP results are in very good agreement with equation (2) for both argon and helium over almost 4 decades in pressure. For the argon CCP simulations at 13.56 MHz there is a large discrepancy for $d/\lambda_\mathrm{i} > 100$, where the simulation h_L is significantly larger; by as much as almost an order of magnitude for $d/\lambda_\mathrm{i} \sim 500$. This discrepancy cannot be explained due to additional ionization in the sheaths from secondary electrons, as demonstrated by the sample points shown (blue stars) where secondaries have been turned off. Although h_L decreases slightly for these points (as expected since less ionization now occurs in the sheaths), there is still a significant discrepancy present. A similar discrepancy also occurs at 60 MHz, and for the helium simulations, in this regime.

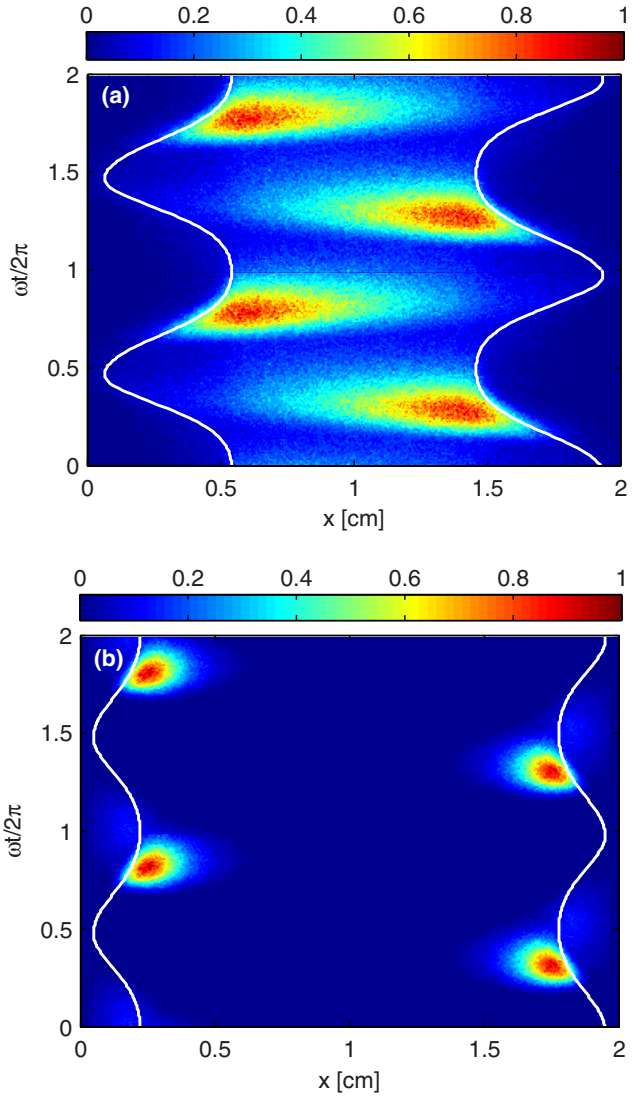

Figure 3. Normalized spatio-temporal ionization rate (over two rf periods) for the argon CCP simulations at 13.56 MHz for (*a*) $d/\lambda_i = 18$ (70 mTorr), and (*b*) $d/\lambda_i = 428$ (1000 mTorr). The white curves show the position of the sheath edge during the rf period.

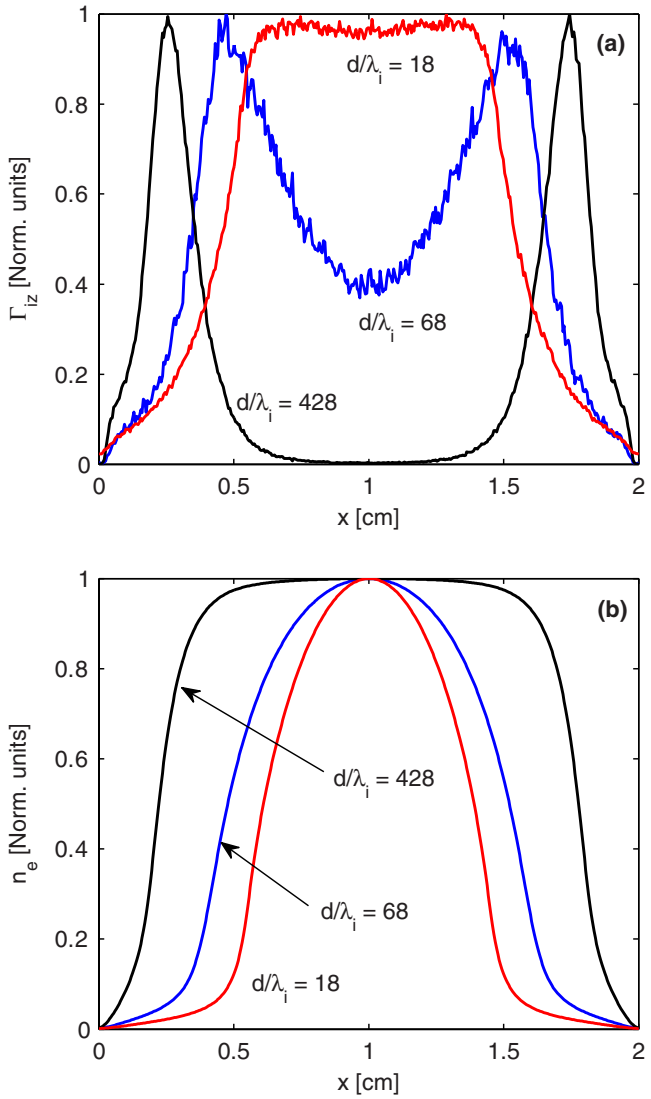

Figure 4. Time-averaged (and normalized) (*a*) spatial ionization rate, and (*b*) electron density, for the argon CCP discharges at $d/\lambda_i = 18$ (70 mTorr), $d/\lambda_i = 68$ (200 mTorr), and $d/\lambda_i = 428$ (1000 mTorr). The applied rf frequency is 13.56 MHz, and $\gamma = 0.1$.

We argue here that the discrepancy between the CCP simulations is related to the more complicated ionization dynamics that occur in these systems, and which are not modeled in equation (2). It is well-known that both the ionization and electron heating rates in CCPs are strongly modulated at the applied rf frequency [42–44]. Significant electron heating occurs when the rf sheaths expand, which can result in a strong modification of the electron distribution function [45], and the formation of electron beams propagating towards the bulk plasma region [44]. These high-energy electrons are very efficient at producing ionization reactions, resulting in a type of ionization front beginning at the sheath edges and propagating inwards to the central plasma. This is well illustrated in figure 3, which shows contour plots of the spatio-temproal ionization rate for the 13.56 MHz argon CCP simulations at $d/\lambda_i = 18$ and $d/\lambda_i = 428$. For low d/λ_i, the mean free path is large and these high energy electrons are able to essentially travel throughout the bulk plasma region (hence producing significant ionization there), while for larger d/λ_i, the mean free path is much shorter and almost no high-energy electrons reach the central region. Hence all ionization is restricted to the near-sheath regions.

The above can also be more easily understood by observing figure 4, which shows normalized profiles of the time-averaged spatial ionization rate and electron density at three conditions: $d/\lambda_i = 18$ (70 mTorr), $d/\lambda_i = 68$ (200 mTorr), and $d/\lambda_i = 428$ (1000 mTorr), for the 13.56 MHz argon CCP simulations. At $d/\lambda_i = 18$ the spatial ionization rate more closely follows the electron density profile, and at this pressure, the simulation h_L is in good agreement with that from equation (2). As the pressure increases however, the ionization profile undergoes a transition, displaying a double-peaked profile, which gets more pronounced as the pressure is increased further. At $d/\lambda_i = 428$ almost no ionization occurs within the bulk plasma, and all ionization now occurs near the sheath edges. This spatial profile now no longer follows the electron density profile, which becomes essentially flat in

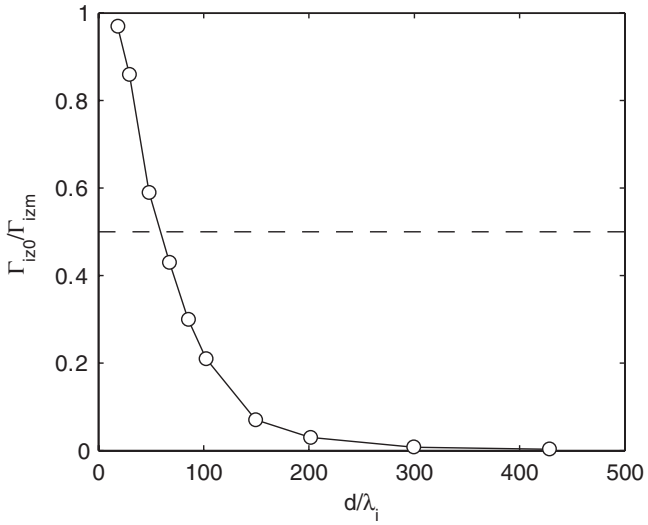

Figure 5. Ratio of the time-averaged ionization rate in the center of the discharge, Γ_{iz0}, to the maximum ionization rate, Γ_{izm}, as a function of d/λ_i for the 13.56 MHz argon CCP simulations. The horizontal dashed line denotes a ratio of 0.5.

the discharge center. Figure 5 shows the ratio of the central ionization rate to the maximum ionization rate as a function of d/λ_i, and we define the bulk-to-sheath edge ionization transition (horizontal dashed line in figure 5) as the value of d/λ_i where the central ionization rate is less than half of the maximum ionization rate. The approximate value of d/λ_i at which this transition occurs is shown as the vertical dashed line in figure 2(*a*), which is seen to be close to where the PIC simulations begin to diverge from equation (2).

For 60 MHz (which is used to allow a discharge to be sustained at lower pressures) a second, but less severe (∼20%), disagreement between simulation and theory occurs at small d/λ_i. Here the simulation h_L is also larger than that predicted by equation (2). At these low values of d/λ_i the discharge is close to extinction, and the bulk plasma region is smaller than, or similar to the sheath width: i.e. we have $d/s \sim 1$. For these simulations, ionization within the sheath (that occurs during sheath expansion for example) effectively increases the ion flux towards the boundaries, and because $d/s \sim 1$, this contribution is more pronounced than at the higher pressures where $d/s > 1$.

We note that the ICP results in figure 2 for both argon and helium are very similar. Because of the transverse heating mechanism used in these simulations, there are no large amplitude rf oscillations in the plasma compared to the CCP simulations, and the plasma potential, electron density, and electron distribution function, are relatively constant throughout the rf period. Hence the ionization rate does not show strong temporal variations, and is more proportional to the electron density profile. In this case the ICP simulations describe a system much closer to the theoretical models [3–5, 30] used as the basis for the calculation of h_L. Consequently these simulations provide a direct validation of the ion transport model used in these theories.

4. Conclusions

In summary, we have explicitly tested the validity and utility of the commonly used formula to estimate the edge-to-center plasma density ratio in single-ion-species, planar, low-temperature discharges. The ICP PIC simulation results are found to be in good agreement over the entire pressure range tested, while the CCP results are found to be in agreement in the intermediate pressure regime. For $d/\lambda_i \gg 1$, a large discrepancy is present, which is correlated with the bulk-to-sheath edge ionization transition that occurs in CCPs at sufficiently high pressures. When this transition occurs, most of the plasma production occurs near the sheath edge, and the ionization rate is no longer proportional to the electron density profile. This transition is not considered in the derivation of equation (2), and has the effect of reducing the effective bulk plasma length, d, and hence increasing the edge-to-center density ratio. At atmospheric pressure it has been shown previously [46] that ionization occurs almost entirely in the sheaths, and thus h_L factors are no longer needed/useful. Therefore, global models used in this regime will significantly underestimate plasma losses to the boundaries. However, as evidenced particularly by the ICP simulation results, the ion transport model used in the derivation of equation (2) seems to be fairly well justified; it is the more complicated spatial variation of the ionization rate (due to spatial and temporal variations in the electron temperature) that appears to be the source of the discrepancy.

It is worth highlighting here that the ICP PIC simulations do not accurately model true ICP discharges. This is because the rf antenna fields cannot be included completely in 1D (and are difficult to include completely even in 2D), and so skin depth effects are not present. Nominally, the rf electric field penetration from an antenna is limited to a thin layer of the order of the skin depth [4, 5], wherein which ohmic and collisionless electron heating can occur. At low pressures, electrons heated within this skin depth layer can travel throughout the discharge before an ionization collision happens. At high pressures though, it can be expected that this ionization will again be more pronounced near the sheath edges. Consequently we anticipate that discrepancies similar to those for CCPs could exist for ICPs in the high pressure regime where $d/\lambda_i \gg 1$. Indeed, by modifying the ICP simulation code to restrict the transverse heating electric field to within a 2.5 cm long region at each boundary (with a zero heating field in the center between these regions), we observe an increase in h_L of about 20–30% for $d/\lambda_i \approx 300$.

Finally, we note that we have only verified equation (2) using 1D simulations. Two-dimensional analytical fluid models [47, 48] of cylindrical discharges have demonstrated that the plasma density profiles show a dependence on the aspect ratio (L/R, where R is the radius) of the discharge, and only for high aspect ratios (>10) do the results coincide with the 1D case.

Acknowledgments

The authors would like to thank Valery Godyak, Allan Lichtenberg, and Mike Lieberman for a number of useful

discussions. This work received financial state aid managed by the Agence Nationale de la Recherche as part of the program 'blanc' under the reference ANR-2011-BS09-40 (EPIC) and the program 'Investissements d'avenir' under the reference ANR-11- IDEX-0004-02 (Plas@Par).

References

[1] Allen J E 2009 *Plasma Sources Sci. Technol.* **18** 014004
[2] Franklin R N 2003 *J. Phys. D: Appl. Phys.* **36** R309
[3] Godyak V A 1986 *Soviet Radiofrequency Discharge Research* (Fall Church, Virginia: Delphic Associates)
[4] Lieberman M A and Lichtenberg A J 2005 *Principles of Plasma Discharges and Materials Processing* (Hoboken, NJ: Wiley)
[5] Chabert P and Braithwaite N 2011 *Physics of Radio-Frequency plasmas* (Cambridge: Cambridge University Press)
[6] Lee Y T, Lieberman M A, Lichtenberg A J, Bose F, Baltes H and Patrick R 1997 *J. Vac. Sci. Technol.* A **15** 113
[7] Lee I, Graves D B and Lieberman M A 2008 *Plasma Sources Sci. Technol.* **17** 015018
[8] Wang Y, Lieberman M A, Wu A C F and Verboncoeur J P 2011 *J. Appl. Phys.* **110** 033307
[9] Cho S and Lieberman M A 2003 *Plasma Sources Sci. Technol.* **12** 244
[10] Chabert P, Raimbault J L, Rax J M and Lieberman M A 2004 *Phys. Plasmas* **11** 1775
[11] Perret A 2004 Effets de la fréquence d'excitation sur l'uniformité du plasma dans les réacteurs capacitifs grande surface *PhD Thesis* Ecole Polytechnique
[12] Chabert P, Raimbault J L, Levif P, Rax J M and Lieberman M A 2005 *Phys. Rev. Lett.* **95** 205001
[13] Hahn Y B and Pearton S J 2000 *Korean J. Chen. Eng.* **17** 304
[14] Thorsteinsson E G and Gudmundsson J T 2010 *Plasma Sources Sci. Technol.* **19** 055008
[15] Corr C S, Gomez S and Graham W G 2012 *Plasma Sources Sci. Technol.* **21** 055024
[16] Lieberman M A and Ashida S 1996 *Plasma Sources Sci. Technol.* **5** 145
[17] Thorsteinsson E G and Gudmundsson J T 2009 *Plasma Sources Sci. Technol.* **18** 045001
[18] Hjartarson A T, Thorsteinsson E G and Gudmundsson J T 2010 *Plasma Sources Sci. Technol.* **19** 065008
[19] Lieberman M A and Boswell R W 1998 *J. Physique* IV **8** 145
[20] Lafleur T, Charles C and Boswell R W 2011 *J. Phys. D: Appl. Phys.* **44** 185204
[21] Porteous R K, Wu H M and Graves D B 1994 *Plasma Sources Sci. Technol.* **3** 25
[22] Goebel D M 2008 *IEEE Trans. Plasma Sci.* **36** 2111
[23] Chabert P, Arancibia Monreal J, Bredin J, Popelier L and Aanesland A 2012 *Phys. Plasmas* **19** 073512
[24] Thorsteinsson E G and Gudmundsson J T 2010 *Plasma Sources Sci. Technol.* **19** 015001
[25] Gudmundsson J T 2002 *J. Phys. D: Appl. Phys.* **35** 328
[26] Kokkoris G, Goodyear A, Cooke M and Gogolides E 2008 *J. Phys. D: Appl. Phys.* **41** 195211
[27] Danko S, Bluhm D, Bolsinger V, Dobrygin W, Schmidt O and Brinkmann R P 2013 *Plasma Sources Sci. Technol.* **22** 055009
[28] Tonks L and Langmuir I 1929 *Phys. Rev.* **34** 876
[29] Schottky W 1924 *Phys. Z.* **25** 635
[30] Raimbault J L and Chabert P 2009 *Plasma Sources Sci. Technol.* **18** 014017
[31] Palacio Mizrahi J H, Gurovich V Tz and Krasik Ya E 2013 *Phys. Plasmas* **20** 032116
[32] Kim G H, Lee H C and Chung C W 2010 *Phys. Plasmas* **17** 073504
[33] Lafleur T and Booth J P 2012 *J. Phys. D: Appl. Phys.* **45** 395203
[34] Lafleur T, Chabert P and Booth J P *Plasma Sources Sci. Technol.* **23** 035010
[35] Turner M M, Derzsi A, Donko Z, Eremin D, Kelly S J, Lafleur T and Mussenbrock T 2013 *Phys. Plasmas* **20** 013507
[36] Baalrud S D, Lafleur T, Boswell R W and Charles C 2011 *Phys. Plasmas* **18** 063502
[37] Phelps A V and Petrović Z Lj 1999 *Plasma Sources Sci. Technol.* **8** R21
[38] Phelps A V 1994 *J. Appl. Phys.* **76** 747
[39] Biagi S F 2004 *Cross section Compilation, version 7.1* see http://www.lxcat.Net
[40] Phelps A V 2005 *Compilation of Atomic and Molecular Data* see http://jila.colorado.edu/ avp/
[41] Godyak V A and Piejak R B 1990 *Phys. Rev. Lett.* **65** 996
[42] Vender D and Boswell R W 1990 *IEEE Trans. Plasma Sci.* **18** 725
[43] O'Connell D, Gans T, Vender D, Czarnetzki U and Boswell R 2007 *Phys. Plasmas* **14** 034505
[44] Schulze J, Heil B G, Luggenhölscher D, Mussenbrock T, Brinkmann R P and Czarnetzki U 2008 *J. Phys. D: Appl. Phys.* **41** 042003
[45] Lafleur T, Boswell R W and Booth J P 2012 *Appl. Phys. Lett.* **100** 194101
[46] Lazzaroni C, Chabert P, Lieberman M A, Lichtenberg A J and Leblanc A 2012 *Plasma Sources Sci. Technol.* **21** 035013
[47] Godyak V and Sternberg N 2008 *Plasma Sources Sci. Technol.* **17** 025004
[48] Sternberg N and Godyak V 2011 *Plasma Sources Sci. Technol.* **20** 015018